-

Probability of Detection and Multi-Sensor Persistence of Methane Emissions from Coincident Airborne and Satellite Observations

Alana K. Ayasse[1], Daniel H. Cusworth[1], Katherine Howell[1], Kelly O'Neill[1], Bradley M. Conrad[2], Matthew R. Johnson[2], Joseph Heckler[3], Gregory P. Asner[3], Riley Duren[1]

[1]Carbon Mapper inc., Pasadena CA
[2]Carleton University, Ottawa ON
[3]Arizona State University, Center for Global Discovery and Conservation Science, Tempe AZ

Abstract

Satellites are becoming a widely used measurement tool for methane detection and quantification. The landscape of satellite instruments with some methane point-source quantification capabilities is growing. Combining information across available sensor platforms could be pivotal for understanding trends and uncertainties in source-level emissions. However, to effectively combine information across sensors of varying performance levels, the probability of detection (POD) for all instruments must be well characterized, which is time-consuming and costly, especially for satellites. In August of 2023, we timed methane-sensing aerial surveys from the Global Airborne Observatory (GAO) to overlap with observations from the NASA Earth Surface Mineral Dust Source Investigation (EMIT). We show how these co-incident observations can be used to determine and verify the detection limits of EMIT and to develop and test a multi-sensor persistence framework. Under favorable conditions the 90% probability of detection at 3 m/s for EMIT is 1060 kg/hr. We further derive a Bayesian model to infer probabilistically whether non-detected emissions were truly off, and we use this model to assess the intermittency of emissions across GAO and EMIT. Time-averaged emission rates from persistent sources can be underestimated if POD is not characterized and if differences in POD across multi-sensor frameworks are not properly accounted for.

Keywords

Methane, EMIT, Remote Sensing, Point Source Emissions, Persistence, Probability of Detection

Synopsis

In this study we coordinated methane-sensing aerial surveys to overlap with observations from a similar satellite instrument in an area with large and frequent methane emissions. We use these data to show how these coordinated observations can be used to determine the detection limits of the satellite instrument and to develop and test a multi-sensor methane plume persistence framework.

Introduction

Reducing methane emissions has received increased attention for addressing global climate change, due to methane's short lifetime and powerful radiative forcing (Etiman et al., 2016;

Ocko et al., 2021). In 2021,150 nations signed the Global Methane Pledge with the goal to reduce emissions 30% by 2030 (Global Methane Pledge). Reducing emissions by this magnitude is both ambitious and critical for achieving global climate targets and requires finding near-term mitigation solutions. In response, and in parallel, to the Global Methane Pledge, efforts to increase monitoring of methane emission sources have been proposed and prototyped, including the UN International Methane Emissions Observatory (IMEO) Methane Alert and Response System (MARS; UNEP 2022), the United States Environmental Protection Agency's updated oil & gas rule (Environmental Protection Agency 2024), including provisions reporting for super-emitting sources (localized emissions above 100 kg CH_4 h^{-1}), the European Union's proposed new methane rule (European Commission 2020), the State of California's new oil&gas rules (Greenhouse Gas Emission Standards for Crude Oil and Natural Gas Facilities 2017), among other regulations and initiatives. Satellites have demonstrated the capability of detecting and quantify methane emissions at the scales relevant to these initiatives (Jacob et al., 2022). Understanding and assessing the performance of satellite technologies is therefore critical for evaluating their ability to address near-term climate goals.

Some passive remote sensing technologies use the shortwave infrared portion of the electromagnetic spectrum for column methane concentration quantification, which can then be used for methane detection for certain classes of high-emitting sources. In particular, one class of passive remote sensing technology, known as imaging spectrometers, measures reflected and backscattered radiance across visible to infrared wavelengths (typically 400-2500 nm) at medium spectral resolution (typically 5-15 nm). There are many imaging spectrometers currently on orbit (PRISMA, EnMAP, EMIT, GaoFen5) that have demonstrated methane sensing and localized super-emitter detection capabilities (Guanter et al. 2021, Roger et al. 2024, Thorpe et al. 2023, He et al. 2023). This paper will specifically focus on the NASA Earth Surface Mineral Dust Source Investigation (EMIT) instrument, onboard the International Space Station (ISS) that has been active since late 2022. EMIT builds on decades of imaging spectrometer development at NASA Jet Propulsion Laboratory, including the Next Generation Airborne Visible/Infrared Imaging Spectrometer (AVIRIS-NG) and the Global Airborne Observatory (GAO), both of which have been leveraged for large scale surveys of super-emitters across oil&gas, solid waste, and livestock sectors (Duren et al., 2019; Cusworth et al., 2022). EMIT, as well as any imaging spectrometer technology, or any other passive remote sensing technology capable of methane detection (e.g., GHGSat, Sentinel-2, LandSat-8, WorldView-3), is limited to detecting a subset of all emission sources. This detection limit is characterized by an instrument's signal-to-noise (SNR) ratio, its spectral resolution, its spatial resolution, and the environmental conditions at the time of observation. For this expanding suite of methane sensing technologies to be used together to understand and reduce methane emissions, the performance, most importantly the detection limit, of these instruments must be well characterized.

Detection limits for remote sensing of methane are typically reported as the Minimum Detection Limit (MDL) or the Probability of Detection (POD). The MDL can be estimated theoretically for an instrument of estimated column measurement precision, spatial resolution, or ground sampling distance (GSD), for certain environmental conditions (Jacob et al. 2016). POD assigns probabilities of detection for an observing system at specific emission rate levels (Conrad et al. 2023). POD is best calculated from real observations, preferably controlled release experiments, where detection for an observing system is evaluated against a wide range of known release rates. Derived POD models from empirical studies are more representative of the true performance of an observing system, including algorithms or manual processes deployed for CH_4 plume detection. However, they require, at minimum, dozens of observations at known release rates, preferably across a set of real-world observing conditions. Controlled release experiments are time consuming and costly to execute, especially for satellites, where observations are typically limited to a single overpass per day, and repeat overpasses are set by an observing system's sample revisit interval.

In addition to different instruments with different detection limits, multiple instruments are now being used in combined multi-scale efforts to assess the total methane impact and persistence of individual facilities (Cusworth et al., 2021; Guanter et al., 2024). Persistence is a metric of how frequently a source emits methane and is crucial for calculating the lifetime methane contribution of a source. By combing data from multiple instruments, we can increase the number of observations of a source and therefore improve persistence characterization. However, when one source is measured at different times by many different instruments with different probabilities of detection it can be difficult to tell if a source has stopped emitting or if the emission is simply being missed by the instrument.

Here we show how to generate a POD model for a satellite instrument (EMIT) efficiently using coincident airborne (GAO) under flights with an airborne instrument whose detection and quantification performance are well characterized. While these coincident observations are still difficult to coordinate, they result in more efficient acquisition of observation samples required to estimate a POD model. We demonstrate an EMIT POD model based on GAO under flights to be consistent with theoretical estimates. This POD model is used to create a new multi-sensor persistence framework from EMIT and GAO observations in the Permian Basin in August of 2023. This framework allows for better probabilistic evaluation of EMIT non-detections for sources where airborne observations showed previous emission activity and shows the importance of POD when analyzing source trends using multiple sensors.

Methods And Data

Data

This study is comprised of data from two imaging spectrometers, EMIT and GAO. Both imaging spectrometers measure radiance between 400 and 2500 nm at roughly 5 nm spectral spacing for GAO and roughly 7 nm for EMIT. GAO has a swath width and pixel size that vary with the altitude of the aircraft; however, for this study the swath width was ~3 km and the pixel size was 5 m. EMIT orbits at about 400 km above Earth's surface. EMIT images are generally 80 km by 80 km and it can collect continuous images along track. The pixel resolution of EMIT can vary depending on the height of the ISS, but is generally 60 m.

On August 20th and 24th 2023, EMIT observed large areas of the Permian Basin and we coordinated GAO observations to coincide with the EMIT overpasses. The Permian Basin is a target rich environment that has reliably been observed with a high density of large, super-emitting methane plumes. It is also a relatively arid region with a homogenous background, little urban development, and few heavily vegetated areas. These conditions make it a good area to test and compare the GAO and EMIT instruments for methane detection. In addition, these conditions are are similar to the conditions where GAO was repeatedly evaluated against blinded controlled releases (Casa Grande, Arizona; El Abbadi et al., 2024).

The field deployment of GAO was designed to ensure that GAO and EMIT observed at least one plume at the same time. Many plumes in the Permian Basin are intermittent (Cusworth et al., 2021); however, there are a few exceptions, including persistent activity at some gas processing plants. To better ensure coincident observation of at least one plume, we targeted a large persistently emitting gas processing plant (31.845285°, -101.77253°) as our primary target. For the hour surrounding the predicted EMIT observation, we repeatedly surveyed this gas processing plant. For the remainder of the flight day, GAO surveyed additional high priority regions within the predicted EMIT observation area. Beyond these co-incident observations, GAO surveyed the same general areas on Aug. 16, 17, 19 and 21. The additional data helped us to identify persistent sources for the EMIT POD assessment described later. Figure 1 shows the EMIT and GAO coverage for the 20th and 24th. In addition, we have detected and quantified plumes observed by EMIT across its observing record.

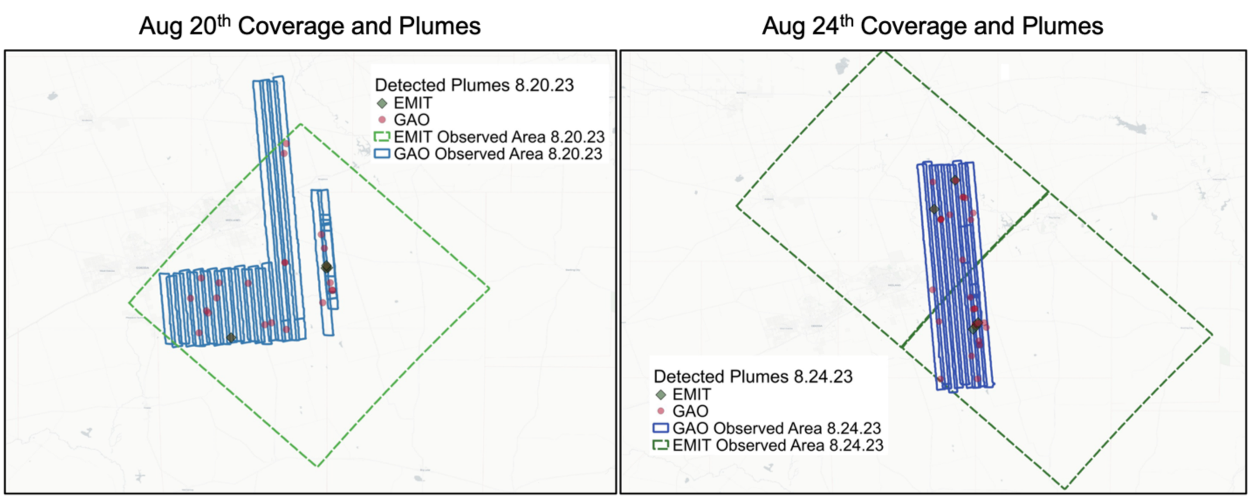

Figure 1. Map of EMIT and GAO coverage on August 20th 2023 (left panel) and August 24th 2023 (right panel) as well as detected plumes.

Methane Emission Detection and Quantification Methods

Both the GAO and EMIT data were processed from radiance data to the methane concentration fields using a columnwise matched filter (Thompson et al. 2015, Foote et al. 2021). Plumes were manually identified by analysts (Carbon Mapper). For GAO, emission rates for each plume were calculated using a concentric circle implementation of the Integrated Mass Enhancement (IME) approach (Duren et al., 2019). In this implementation the IME is calculated iteratively with an expanding radial fetch distance and then averaged across a set of radii starting near the plume's origin until the plume's radial terminal point, or until a maximum fetch of 285 m is reached. Variability in wind estimates and in length normalized IME across radial iterations is propagated to emission rate uncertainty. This GAO quantification approach has been shown to provide results that are correlated and in aggregate unbiased with metered emission rates in controlled release experiments (El Abbadi et al., 2024).

For EMIT we build on the approach introduced in Thorpe et al (2023). Specifically, we calculate the IME of all plume pixels starting from the plume origin and extending to the plume's terminal radial point or maximum fetch of 2500 m. Source emission rate is quantified by dividing this IME by the fetch and multiplying the by 10-m wind speed. Uncertainties in wind, IME, and plume length are all propagated to the total emission rate. IME uncertainty is the sum of retrieval and delineation uncertainties, which are derived from the variability in retrieved local background concentrations and the IME variability across plume delineations at fixed L. Length uncertainty is a function of pixel size. The wind uncertainty is the variability in space, which is calculated using the standard deviation from a 9 km window around the source location, and time, which is the standard deviation from a 3 hour window surrounding the plume. For both instruments the wind products used for this analysis came from High Resolution Rapid Refresh (HRRR) 10 m wind product (Dowell et al. 2022).

At the time of this study, no quantification algorithm applied to EMIT has been rigorously tested with controlled releases, however, Figure 2 shows the results of three simultaneous EMIT and GAO detections spaced less than three minutes apart. The GAO and EMIT plume observed 1.4 min apart on Aug. 20th (08.20.23-A) show good agreement on both the shape of the plume and the derived emission rates. On Aug. 24th both GAO and EMIT independent detections were observed 2.8 min apart. Source 08.24.23-B also shows close agreement between GAO and EMIT, while source 08.24.23-A shows some discrepancy between GAO and EMIT. The discrepancy could be due to variable wind speeds, even under near simultaneous observation, the shapes of the plumes for source 08.24.23-A suggestion changing wind directions between GAO and EMIT overpasses.

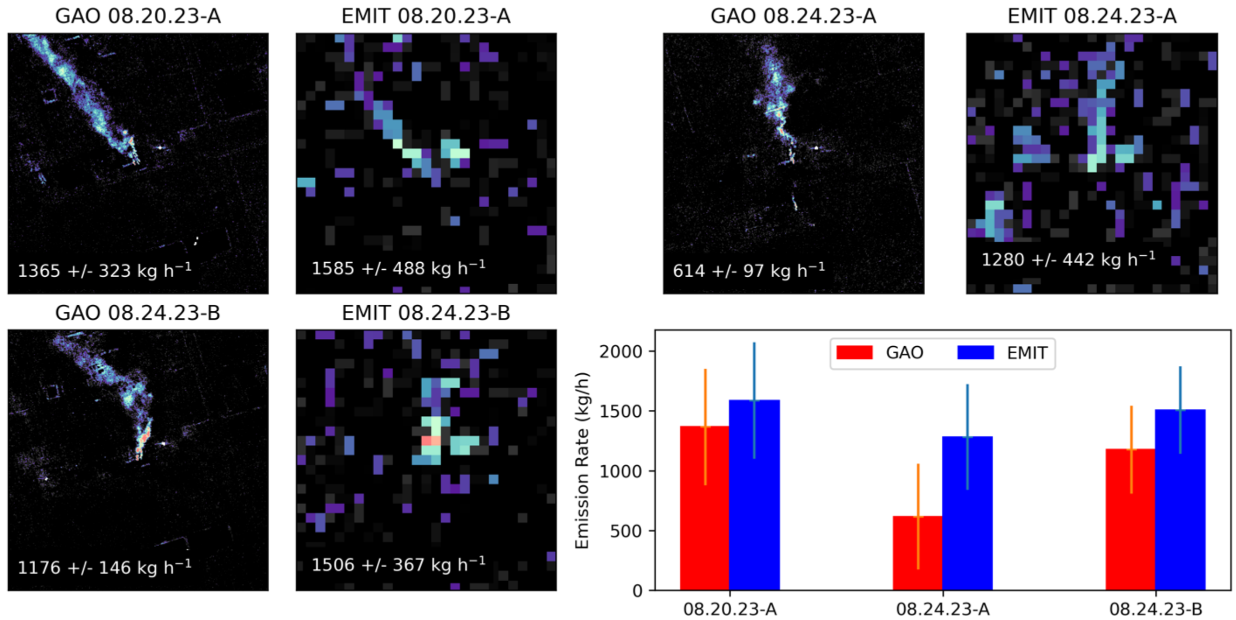

Figure 2. The images are methane concentration images (matched filter outputs) from EMIT and GAO for the three plumes measured with in 3 minutes of one another. The emission rate for each plume is included on the image as well as displayed on the bar chart on the bottom right.

An additional six plumes were detected and quantified between GAO and EMIT on Aug 20th and 24th, though with more temporal spacing. This resulted in large difference in quantified emission rates between GAO and EMIT overpasses (Figure 3).

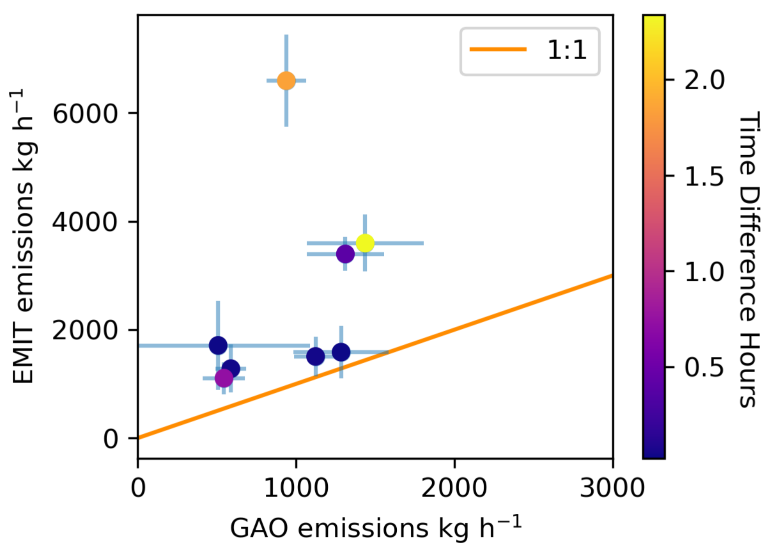

Figure 3. Parity plot between GAO and EMIT for sources measured on the same day by each instrument. The points are colored by the time difference between the GAO and EMIT observation.

This discrepancy may be due to variability of individual sources. For example, Figure 4 shows results of GAO emission quantification at the targeted gas processing plant that was observed on

Aug 20th by GAO (5 times within a 40-minute period) and EMIT and again by just GAO on August 25th (8 times within a 60-minute period). On the 20th, quantified emission rates by GAO varied as much as 28% within 12 minutes. On the 24th, quantified emission rates varied as much as 43% in 11 minutes. Emissions over time, even short periods of time, can vary therefore only observations that are at nearly the exact same time are useful for direct comparison.

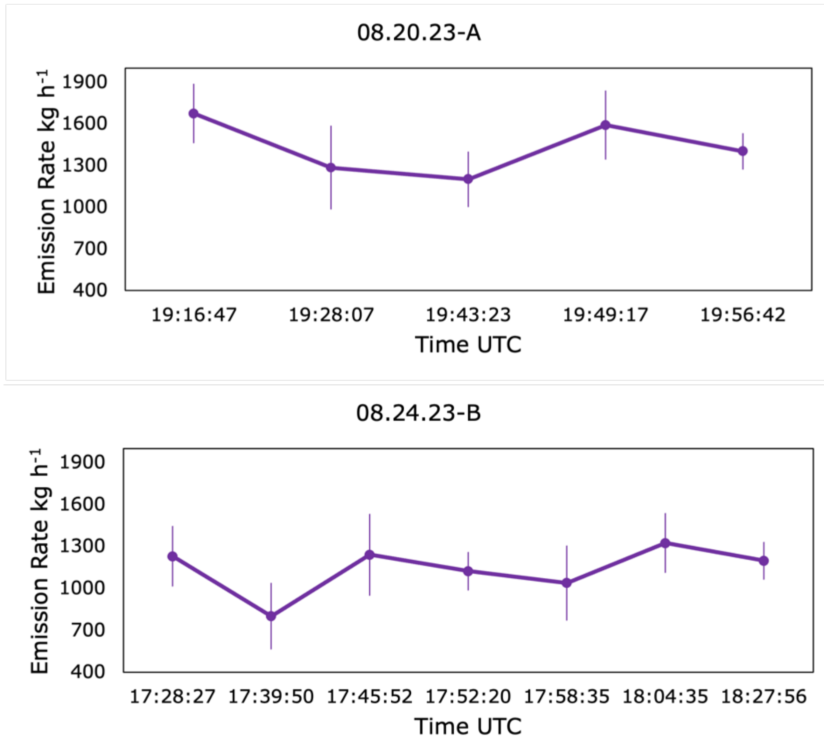

Figure 4. Emission rate time series from multiple GAO observations at the targeted gas processing plant on Aug. 20th and Aug. 24th 2023.

Results and Discussion

Probability of Detection

POD is generally empirically estimated using a sampling of plumes that are above, at, and below the detection limit of the instrument using controlled emission releases (Conrad et al., 2023). Though not a controlled test environment, on Aug 20th and 24th GAO and EMIT were able to sample a distribution of plumes that were above and below EMIT's detection limits (Figure 5). However, while we had very close to simultaneous acquisitions over our main target, for the rest of the area surveyed by GAO there could be as much as a 3-hour time difference between when a source was observed by GAO and EMIT. This time difference can make a direct comparison of emission rates challenging, but for POD we can tolerate higher emission rate variability if the emissions are significantly above or below the detection limit. For observations near the detection limit we may be incurring some error due to time variability and this error will have to be corrected for as more data become available. Sources can also be highly intermittent even within a few hours, therefore we selected sources where we had high confidence of continuous emission for the duration of the campaign. High confidence in source persistence is critical for classifying EMITs non-detections resulting from the detection limit and not due to potential short-duration emission events. To build this confidence in persistence, we used GAO data collected on August 16th, 17th, 19thand 21st that covered roughly 1900 km^2 or 15-30 % of the EMIT area. If the source was emitting on all overpasses and has at least three overpasses then we considered the source to be persistent and we assumed the source was emitting at the time of the EMIT acquisition. If the source was only present in one image, then we considered that source to be intermittent and excluded it from the probability of detection analysis. Some sources had multiple overpasses by GAO on the 20th and 24th, for these sources we use the emission estimate that is closest in time to the EMIT acquisition. This left us with a total of 55 detected plumes at sources identified by GAO, 9 of which were detected by EMIT and 46 missed by EMIT (Figure 5).

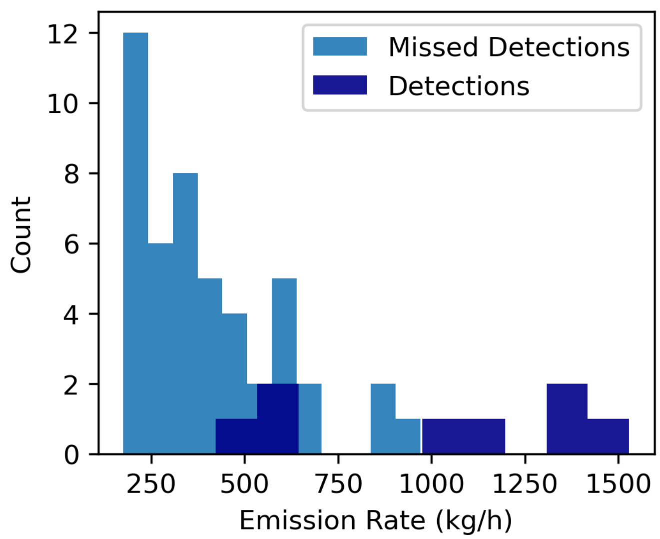

Figure 5. Detection and missed detection by EMIT from the coincided GAO/EMIT acquisition. The detects/missed detects are binned by emission rate.

POD is the probability that an instrument, retrieval, and detection algorithm detects a methane plume given the emission rate, the wind speed, the solar and albedo properties of the location, and the instrument properties. This can be summed up in theoretical model developed by Conrad et. al., 2023 (here after referred to as Conrad et.al.) that takes the following form:

$$x = \Phi_7 * \frac{(Q - \Phi_1)^{\Phi_3}}{(h)^{\Phi_5} * (U - \Phi_2)^{\Phi_6}} \tag{1}$$

$$P = 1 - \left(1 + (x^2)\right)^{-1.5} \tag{2}$$

where Q is the emission rate, h is the pixel resolution, and U is the wind speed. Φ is used to denotate coefficients that will be optimized from the EMIT and GAO data. Signal-to-Noise Ratio

(SNR), which is determined by a combination of instrument properties, solar zenith angle, and the surface albedo, can be added to the denominator as N^{ϕ_4}. However, given that SNR did not vary in our study this parameter is not used in the calculations. Equation 2 is the inverse link function, which is specified here as the Burr cumulative distribution function (CDF) but more generally could be the CDF of any distribution with non-negative support (Conrad et al. 2023).

We optimized the coefficients by minimizing *l* in the following equation:

$$l(\phi,\theta) = \sum_i -(D_i \ln F_i + (1 - D_i)\ln(1 - F_i)) \tag{3}$$

where ϕ and θ are a pair of predictor and inverse link functions respectively. In this case ϕ is equation 1 and θ is equation 2. D_i represents a successful detect (1) or a missed detect (0) by EMIT for every GAO observation (i). F_i is the output of the predictor and inverse link function for a given GAO observation (i). The final form of the POD model for EMIT resulted in the following equation with the inverse link function (equation 2):

$$x = .0138 * \frac{(Q + .00379)^{1.97}}{(h)^{1.97} * (U + .00064)^{0.88}} \tag{4}$$

We also looked at alternative models from Conrad et. al. and found little substantive difference in the predicted probabilities.

We find that at a 3 m/s wind speed the 90% POD is 1060 kg/hr (Figure 6). This is consistent with what we have observed by analyzing a global distribution of emission rates quantified with EMIT. The most frequent emission rate range for windspeeds below 4 m/s in all plumes collected and processed by Carbon Mapper from EMIT data, is 900-1200 kg/hr (figure 7). If we assume that emission rates follow a power law (Sherwin et al., 2024), then we can assume that the point just past the peak of the histogram is the 90% POD and all emissions below the peak are not representative of the true distribution of emissions but rather the partial detection limit of the instrument. The good agreement between the modeled 90% POD and the observed emission peak indicates that the model is likely representative of the performance of the instrument. The theoretical minimum detection assumptions from Jacob et. al. 2016 predicts the MDL to be 244 kg/hr for a 3 m/s wind speed. We find that this emission rate results in a 2% POD, which is to be expected as the MDL represents the theoretical bottom limit. While this POD model aligns with independent methods, we do caution that the concentration and detection methods and the limited sample size may affect its global applicability. Methane concentration retrievals methods and plume detection methods can also affect the POD. The POD presented here is only applicable within the methods presented in this paper; a different set of detection methods applied to the EMIT instrument could result in a different POD estimate. In addition, the small amount of data and the limited geography of these data may bias the results and a larger and more diverse data set is crucial to creating a better constrained model. However, this analysis demonstrates how these types of data can be used to characterize the performance of satellite instruments when controlled release data is not available.

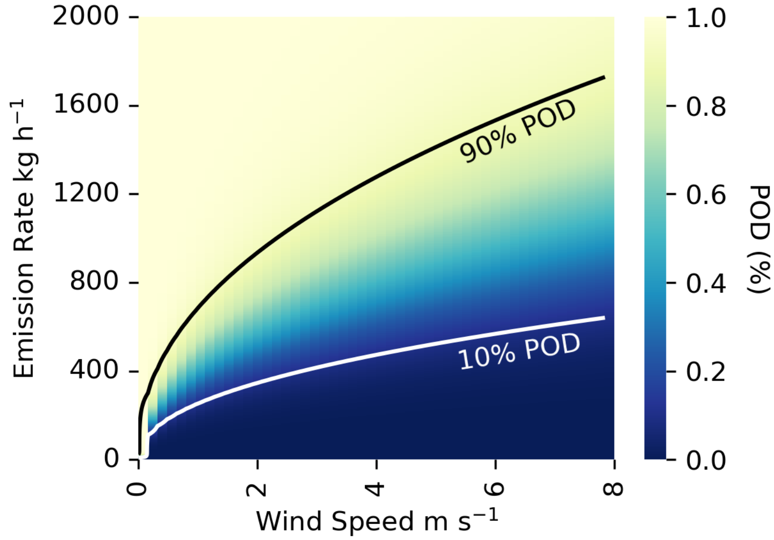

Figure 6. POD heat map for EMIT, windspeed is on the x-axis, emission rate on the y-axis, and the colors represent the POD. The 90% POD and 10% POD line are displayed for reference on the figure.

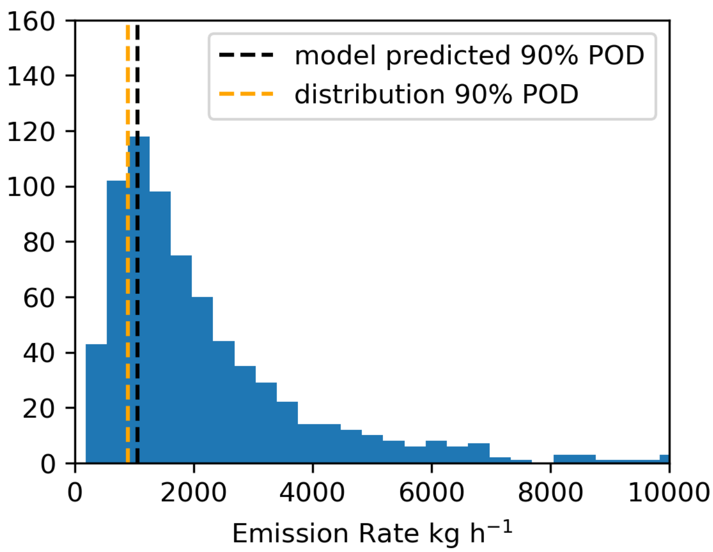

Figure 7. Distribution of all quantified methane emission from EMIT under 4 m/s windspeeds at time of analysis (n = 735, bins = 50). The Model predicated 90% POD is the 90% POD at 3 m/s that comes from the model in equation 4. The distribution 90% POD is where we estimate the EMIT distribution starts to diverge from a theoretical true distribution.

Assessing persistence using multiple sensors

Persistence, or plume detection frequency at the source level, is a key metric for understanding and quantifying methane emissions. Persistence provides information on how frequently a given source or area likely needs observation to reliably detect a plume and it helps us to quantify the total methane contribution of a source. A large plume from a highly intermittent source may contribute less methane than a small but persistent source over the sources' lifetimes. Calculating persistence becomes acutely difficult for multi-sensor applications with varying POD characteristics. For example, a persistently emitting facility at a low emission rate, may be detected by a low detection limit instrument, but not a high detection limit instrument. Not accounting for instrument differences would bias persistence estimates for that theoretical facility.

We propose a prototype multi-sensor persistence algorithm, based on empirical POD information using Bayesian inference. Calculating multi-sensor persistence requires decomposing the number of instrument overpasses (N) into two components: overpasses that can be used to conclusively calculate persistence (N_c) overpasses that cannot be used to conclusively calculate persistence (N_N), where $N = N_c + N_N$. N_N includes overpasses where observations may have been obscured (e.g., cloudy scenes), but may also include overpasses where one lacks confidence that a non-detection truly captured reality (i.e. the non-detect was due to detection limits rather that a source that stopped emitting). This lack of confidence can be estimated probabilistically: here the goal is to estimate the probability that a source is emitting CH4 (on) given that an observation was made without a detection (-), here written as $\underline{p(\,on\,|-\,)}$. Using Bayes's Theorem, this is explicitly estimated using the following form:

$$p\ (on\ |-) = \frac{p(-\mid on\ )\,p(on)}{p(-\mid on\ )\,p(on)\ +\ p(-\mid off\ )\,p(off)} \tag{5}$$

where $p(-\mid on\ )$ represents the probability of not detecting a source that is emitting. This value is estimated using an empirical POD curve derived for an instrument using Equations 1 and 2:

$$p(-\mid on\ ) = 1 - POD^{I}(q^{*}, u) \tag{6}$$

where POD^{I} represents a unique POD function for instrument I, and q^{*} is a representative emission rate for the emitting source. This value would ideally be the emission rate at the time of observation. However, in practice it is impossible to estimate this value given that the observation resulted in no detection. Instead, one can assume this value, possibly using a distribution of previously estimated emission rates at that source. The value $p(-\mid off\ )$ represents the probability of not detecting a source that is off. This value can be estimated by the true negative rate (TNR), which is a function of true negative (TN) and false positive (FP) detections, derived from controlled release or other validation experiments:

$$TNR = \frac{TN}{TN + FP} \tag{7}$$

The values $p(on)$ and $p(off)$ represent prior probabilities that an emission source is emitting or not, respectively.

Assumptions on prior probability distributions influence estimation of $p\ (on\ |-)$. We show two applications of this framework under differing assumptions for $p(on)$. First, we assume $p(on)$ to be emission persistence (f^*) of that source derived from previous overflights, assuming at least 3 previous overpasses with GAO: f^* = M/N, where M = number of detections and N = number of overpasses from previous airborne overpasses. The value $p(off)$ is then estimated as 1-f^*. Using these assumptions, $p\ (on\ |-)$ reduces to the following form:

$$p\ (on\ |-) = \frac{\left(1 - POD^I(\bar{\mathbf{q}}, u)\right)(f^*)}{\left(1 - POD^I(\bar{\mathbf{q}}, u)\right)(f^*) + TNR(1 - f^*)} \tag{8}$$

Multi-sensor persistence is then estimated using Equation 8 and the following algorithm:

Algorithm 1
If airborne observations at a source satisfy $N_c > 3$;
    For observation i=N+1 of instrument I at a source:
        Set $f_{i-1}^* = \frac{M}{Nc}$
        Set $q^* = \bar{\mathbf{q}}$
        Compute $p\ (on\ |-) = \frac{(1-POD^I(q^*,u))(f_{i-1}^*)}{(1-POD^I(q^*,u))(f_{i-1}^*)+TNR(1-f_{i-1}^*)}$
        If $p\ (on\ |-) < 0.5$:
            $Nc = Nc + 1$
        Else
            $N_N = N_N + 1$
        $f_i^* = \frac{M}{Nc}$
Else:
    No persistence estimate can reliably be computed.

Second, we assume $p(on)$ as the probability defined by an autocorrelative model. Here, this underlying assumption is that the most recent previous observation at that source is most predictive of the sources current on/off state. We assume an autocorrelative model of the following form:

$$X_t = a + bX_{t-1} + c\lfloor\overline{(X_{t-2}, \dots, X_N)}\rceil \tag{9}$$

where X represents the binary outcome of whether a plume was detected at some time of observation $t \in [1, \dots, N]$. Values a, b, c represent regression coefficients, and $\lfloor\bullet\rceil$ represents a rounding operation. We fit the coefficients of this model using source-level observations from previous airborne campaigns in the Permian Basin (Cusworth et al., 2022). When trained on the entire dataset, we find fair predictive ability of this model to estimate the “on” state of a source, with precision of 0.73, recall of 0.79, and f-1 score of 0.76. We assume $p(on)$ to be the predicted probabilities from the logistic regression model. There are only 4 permutation of model states that exist in Equation 10 given the state of the previous overpass (t_{-1}) and overpasses prior to that (t_{-2+}). Let $\varphi(t_{-1}, t_{-2+})$ be the function that maps previous overpass states to probabilities, then $\varphi(t_{-1}, t_{-2+})$ takes the following form:

$$\varphi(t_{-1}, t_{-2+}) = \begin{cases} 0.72 & \text{if } t_{-1} = 1 \text{ and } t_{-2+} = 1 \\ 0.65 & \text{if } t_{-1} = 1 \text{ and } t_{-2+} = 0 \\ 0.26 & \text{if } t_{-1} = 0 \text{ and } t_{-2+} = 1 \\ 0.19 & \text{if } t_{-1} = 0 \text{ and } t_{-2+} = 0 \end{cases} \quad (10)$$

Therefore, the most recent previous overpass is the largest driver in the proximal state of emission for the source. Using these explicit probabilities, the multi-sensor persistence algorithm takes the following form:

Algorithm 2
If airborne observations at a source satisfy $N_c > 2$;
  For observation $i=N+1$ of instrument I at a source:
    Set $q^* = \bar{\mathbf{q}}$
    Compute $p\ (on\ |-) = \frac{(1-POD^I(q^*,u))(\varphi(t_{-1},t_{-2+}))}{(1-POD^I(q^*,u))(\varphi(t_{-1},t_{-2+}))+TNR(1-\varphi(t_{-1},t_{-2+}))}$
    If $p\ (on\ |-) < 0.5$:
      $N\mathrm{c} = N\mathrm{c} + 1$
    Else
      $N_N = N_N + 1$

Else:
  No persistence estimate can reliably be computed.

Persistence can impact emissions at a facility or source scale and at a basin scale. In figure 8 we show an example of 2 sources that were observed by EMIT on the Aug 24th but where no plume was detected. One source is truly 'off' (Figure 8, source 2) and the other is 'on' but below the EMIT detection limit (Figure 8, source 1). Source 1 was observed 4 times by GAO between Aug 17 and Aug 21, and plumes were observed 3 of the 4 times, yielding a persistence of 75%. On Aug. 24th, if we assume EMIT was the only observation, a simple persistence would lead us recalculate the persistence to be 60% however if we consider the emission rate (q^* = 227 kgh^{-1}) from the previous airborne observations and the wind speed at the time of the EMIT observation (u = 5 ms^{-1}), Equation 4 tells us the POD for EMIT at this source is 1%. Given the POD and the prior persistence (f^* = .75) this yields a probability $p\ (on\ |-)$ > 0.5, meaning that N_N and not Nc was incremented. Therefore, this non-detect was not conclusive enough to make the determination that the source was truly not emitting. This results in the source persistence remaining at 75%. We can confirm this result with the GAO observations from Aug 24th that show the source was indeed emitting but below the EMIT detection limit. Source 2 shows an example of an airborne detection that had a higher emission estimate (q* = 4217 kgh^{-1}), if the source had been emitting, Equation 4 tells us that the POD for EMIT would be 99%. In this case, given the prior persistent (f^* = .25), $p\ (on\ |-)$ < 0.5, providing more confidence that this non detection truly represented the state of this source, so Nc was incremented the persistence is adjusted to 20%. Again, we can confirm this result with the GAO observations that shows the source was not emitting on this day. For the two examples described above, because they are extreme examples, the autocorrelation prior approach results in the same persistence as the standard simple prior Bayesian persistence.

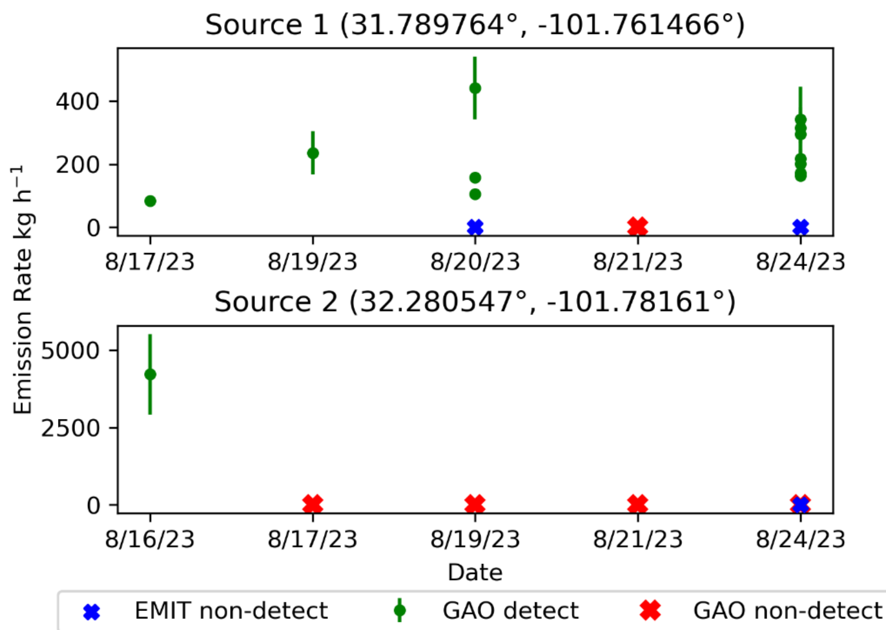

Figure 8. Time series of two example sources from the GAO/EMIT dataset. Both include EMIT non-detects however for Source 1 the EMIT non-detects are due to EMIT's detection limit and for Source 2 the EMIT non-detect is due to the source no longer emitting. This distinction is critical for understanding source/facility level methane emission dynamics.

The multi-sensor Bayesian approach (regardless of prior choice) for updating persistence will always result in higher persistence estimation than using a straight detection frequency as some non-detects will be considered inconclusive. This is shown clearly in the right panel of Figure 9. However, the choice of prior can also impact the persistence estimation across a large population of sources. The autocorrelation prior (Bayesian multi-sensor persistence with an autocorrelation weighted prior) approach results in higher persistence across the whole population compared to the simple persistence approach (Figure 9). In general, the Autocorrelation approach is less likely to assume confidence in the EMIT non-detects and therefore the autocorrelation prior approach is more like the airborne only persistence (i.e. what would happen if we excluded EMIT entirely). However, where the Autocorrelation approach has confidence in the EMIT non-detects, the sample size increases and provides more confidence in the persistence estimate than the aircraft data alone. The standard Bayesian simple prior (Bayesian multi-sensor persistence with a simple persistence prior) approach is more likely to assume confidence in the EMIT non-detects especially for prior intermittent sources ($f^* < 0.5$) and therefore has the largest effect on persistent sources.

For the data within our study, we show that not accounting for POD when calculating persistence leads to an underestimate in the total emission estimate, particularly from small persistent sources. In the left panel of Figure 9, we show the total persistence adjusted emission rate for all sources in this study using the simple persistence approach, the multi-sensor persistence approaches, and airborne alone (excluding EMIT data). The simple persistence has a 11% underestimate compared the Autocorrelation approach and a 6% underestimate compared to the standard Bayesian approach. Most of this underestimate comes from the small persistent sources. The aircraft data alone shows the highest total emission rates but also has the fewest number of samples per-source and therefore we have lower confidence in the persistence estimates. This study only represents a short time period of time (< 1 month) but if you extrapolate out quarterly or annually, and include more EMIT data, the underestimate of the methane emission contribution from persistent sources would become significantly larger. Therefore, when assessing facility or basin scale emissions using data from multiple sensors it is crucial that the POD for each sensor be well characterized, and the proposed multi-sensor persistence framework be adopted to characterize persistence.

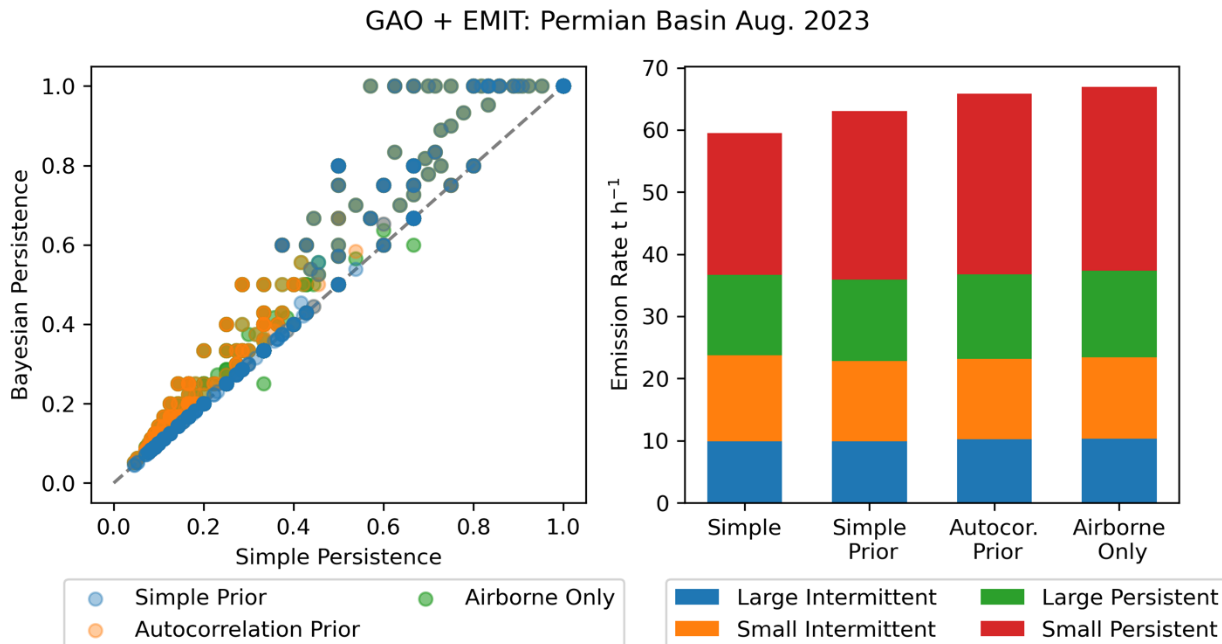

Figure 9. The left panel shows the simple persistence on the x-axis for all sources. On the y-axis are the two Bayesian models (simple prior and autocorrelation prior) and the Airborne Only (no EMIT data) persistence. The right panel shows the total persistence adjusted emission rate for all sources within the study using the 4 different persistence estimation methods from left panel. For each bar the total emission is broken out by large intermittent (q>700 kg/hr, f <0.5), Small intermittent (q<700 kg/hr, f <0.5), Large persistent (q>700 kg/hr, f >0.5) and Small persistent (q<700 kg/hr, f >0.5).

Conclusion

We use two days of coincident EMIT and GAO observations to identify the POD for EMIT, verify the EMIT emission rates, and demonstrate a multi-scale persistence framework. We show that under good conditions the 90% POD of EMIT at 3 m/s wind speed is 1060 kg/hr. While we find generally good agreement between the coincident GAO and EMIT observations, the variability in emissions over time complicates direct comparisons with a small number of measurements. We stress the need for robust controlled release experiments to fully validate the EMIT emissions estimates.

We also introduce a Bayesian approach for determining source persistence when using multiple sensors with different detection limits. Our coincident data provided a unique dataset with which to test and verify the accuracy of this framework. We show that by adopting the multi-sensor Bayesian approach we avoid underestimating emissions, particularly smaller persistent emissions. Going forward these methods could enable quantification of both basin and facility level emissions and persistence with multiple instruments, provided that each instrument has a well-characterized POD. This framework is increasingly necessary as the number of methane sensing instruments grows. In the coming year more remote sensing technologies are scheduled to come online including Carbon Mapper and MethaneSat (Zandbergen et al. 2022, Hamburg et al. 2022). In addition to satellites there are, and will continue to be, airborne instruments mapping methane plumes. For this expanding suite of methane sensing technologies to be used together to understand and reduce methane emissions, the probability of detection of these instruments must be well characterized and methods to accurately integrate the data, like the proposed multi-sensor persistence estimation method, must be adopted.

Acknowledgments

We would like to acknowledge the EMIT Science team including Philip Brodrick, Andrew Thorpe, and Clayton Elder for help with the EMIT forecast. From the Carbon Mapper team, we would like at acknowledge Andrew Aubrey, Ralph Jiorle, and Deja Newton for supporting the GAO flights and data. We would like to thank the GAO team for flight operations. The Global Airborne Observatory (GAO) is managed by the Center for Global Discovery and Conservation Science at Arizona State University. The GAO is made possible by support from private foundations, visionary individuals, and Arizona State University. Funding for flight operations and/or data analysis referenced in this paper was supported by NASA Carbon Monitoring System and the Earth Surface Mineral Dust Source Investigation (EMIT) Science and Applications Team. Lastly, the Carbon Mapper team acknowledges the support of their sponsors including the High Tide Foundation, Bloomberg Philanthropies, Grantham Foundation, and other philanthropic donors.

References

Carbon Mapper. *Carbon Mapper Quality Control Description Document.* https://carbonmapper.org/wp-content/uploads/2023/10/Carbon-Mapper-Plume-Dection-Quality-Control-Public.pdf. (accessed 2024-06-04).

Conrad, B. M.; Tyner, D. R.; Johnson, M. R. Robust Probabilities of Detection and Quantification Uncertainty for Aerial Methane Detection: Examples for Three Airborne Technologies. *Remote Sens. Environ*. **2023**, 288 (113499), 113499.

Cusworth, D. H.; Duren, R. M.; Thorpe, A. K.; Olson-Duvall, W.; Heckler, J.; Chapman, J. W.; Eastwood, M. L.; Helmlinger, M. C.; Green, R. O.; Asner, G. P.; Dennison, P. E.; Miller, C.

E. Intermittency of Large Methane Emitters in the Permian Basin. *Environmental Science & Technology Letters* **2021**. https://doi.org/10.1021/acs.estlett.1c00173.

Cusworth, D. H.; Thorpe, A. K.; Ayasse, A. K.; Stepp, D.; Heckler, J.; Asner, G. P.; Miller, C. E.; Yadav, V.; Chapman, J. W.; Eastwood, M. L.; Green, R. O.; Hmiel, B.; Lyon, D. R.; Duren, R. M. Strong Methane Point Sources Contribute a Disproportionate Fraction of Total Emissions across Multiple Basins in the United States. *Proceedings of the National Academy of Sciences* **2022**, 119 (38), e2202338119.

Dowell, D. C.; Alexander, C. R.; James, E. P.; Weygandt, S. S.; Benjamin, S. G.; Manikin, G. S.; Blake, B. T.; Brown, J. M.; Olson, J. B.; Hu, M.; Smirnova, T. G.; Ladwig, T.; Kenyon, J. S.; Ahmadov, R.; Turner, D. D.; Duda, J. D.; Alcott, T. I. The High-Resolution Rapid Refresh (HRRR): An Hourly Updating Convection-Allowing Forecast Model. Part I: Motivation and System Description. *Weather Forecast*. **2022**, 37 (8), 1371–1395.

Duren, R. M.; Thorpe, A. K.; Foster, K. T.; Rafiq, T.; Hopkins, F. M.; Yadav, V.; Bue, B. D.; Thompson, D. R.; Conley, S.; Colombi, N. K.; Frankenberg, C.; McCubbin, I. B.; Eastwood, M. L.; Falk, M.; Herner, J. D.; Croes, B. E.; Green, R. O.; Miller, C. E. California's Methane Super-Emitters. *Nature* **2019**, 575 (7781), 180–184.

El Abbadi, S. H.; Chen, Z.; Burdeau, P. M.; Rutherford, J. S.; Chen, Y.; Zhang, Z.; Sherwin, E. D.; Brandt, A. R. Comprehensive Evaluation of Aircraft-Based Methane Sensing for Greenhouse Gas Mitigation. 2023.

Environmental Protection Agency. *Standards of Performance for New, Reconstructed, and Modified Sources and Emissions Guidelines for Existing Sources: Oil and Natural Gas Sector Climate Review. Federal Register.* https://www.federalregister.gov/documents/2024/03/08/2024-00366/standards-of-performance-for-new-reconstructed-and-modified-sources-and-emissions-guidelines-for (accessed 2024-05-09).

Etminan, M.; Myhre, G.; Highwood, E. J.; Shine, K. P. Radiative Forcing of Carbon Dioxide, Methane, and Nitrous Oxide: A Significant Revision of the Methane Radiative Forcing. *Geophys. Res. Lett.* **2016**, 43 (24). https://doi.org/10.1002/2016gl071930.

European Commission. *Communication on an EU strategy to reduce methane emissions COM(2020) 663 final. COMMUNICATION FROM THE COMMISSION TO THE EUROPEAN PARLIAMENT, THE COUNCIL, THE EUROPEAN ECONOMIC AND SOCIAL COMMITTEE AND THE COMMITTEE OF THE REGIONS on an EU strategy to reduce methane emissions.* https://eur-lex.europa.eu/legal-content/EN/TXT/?uri=CELEX%3A52020DC0663 (accessed 2024-05-09).

Foote, M. D.; Dennison, P. E.; Sullivan, P. R.; O'Neill, K. B.; Thorpe, A. K.; Thompson, D. R.; Cusworth, D. H.; Duren, R.; Joshi, S. C. Impact of Scene-Specific Enhancement Spectra on Matched Filter Greenhouse Gas Retrievals from Imaging Spectroscopy. *Remote Sens. Environ*. **2021**, 264, 112574.

Global Methane Pledge. https://www.globalmethanepledge.org (accessed 2024-02-07).

Greenhouse Gas Emission Standards for Crude Oil and Natural Gas Facilities; 2017. https://ww2.arb.ca.gov/resources/documents/oil-and-gas-regulation.

Guanter, L.; Irakulis-Loitxate, I.; Gorroño, J.; Sánchez-García, E.; Cusworth, D. H.; Varon, D. J.; Cogliati, S.; Colombo, R. Mapping Methane Point Emissions with the PRISMA Spaceborne Imaging Spectrometer. *Remote Sens. Environ*. **2021**, 265 (112671), 112671.

Guanter, L.; Roger, J.; Sharma, S.; Valverde, A.; Irakulis-Loitxate, I.; Gorroño, J.; Zhang, X.; Schuit, B. J.; Maasakkers, J. D.; Aben, I.; Groshenry, A.; Benoit, A.; Peyle, Q.; Zavala-Araiza, D. Multi-Satellite Data Depicts Record-Breaking Methane Leak from a Well Blowout. 2024.

Hamburg, S.; Gautam, R.; Zavala-Araiza, D. MethaneSAT - A New Tool Purpose-Built to Measure Oil and Gas Methane Emissions from Space. *ADIPEC, Abu Dhabi. SPE.* **2022**. https://doi.org/10.2118/210922-ms.

He, Z.; Gao, L.; Liang, M.; Zeng, Z.-C. A Survey of Methane Point Source Emissions from Coal Mines in Shanxi Province of China Using AHSI on Board Gaofen-5B, 2023. https://doi.org/10.5194/egusphere-2023-3047.

Jacob, D. J.; Turner, A. J.; Maasakkers, J. D.; Sheng, J.; Sun, K.; Liu, X.; Chance, K.; Aben, I.; McKeever, J.; Frankenberg, C. Satellite Observations of Atmospheric Methane and Their Value for Quantifying Methane Emissions. *Atmos. Chem. Phys*. **2016**, 16 (22), 14371–14396.

Jacob, D.J.; Varon, D.J.; Cusworth, D.H.; Dennison, P.E.; Frankenberg, C.; Gautam, R., Guanter, L.; Kelley, J.; McKeever, J.; Ott, L.E.; Poulter, B. Quantifying methane emissions from the global scale down to point sources using satellite observations of atmospheric methane. *Atmospheric Chemistry and Physics*. **2022**, *22*(14), 9617-9646.

Jervis, D.; McKeever, J.; Durak, B. O. A.; Sloan, J. J.; Gains, D.; Varon, D. J.; Ramier, A.; Strupler, M.; Tarrant, E. The GHGSat-D Imaging Spectrometer. *Atmos. Meas. Tech*. **2021**, 14 (3), 2127–2140.

Johnson, M. R.; Tyner, D. R.; Szekeres, A. J. Blinded Evaluation of Airborne Methane Source Detection Using Bridger Photonics LiDAR. *Remote Sens. Environ*. **2021**, 259 (112418), 112418.

Ocko, I. B.; Sun, T.; Shindell, D.; Oppenheimer, M.; Hristov, A. N.; Pacala, S. W.; Mauzerall, D. L.; Xu, Y.; Hamburg, S. P. Acting Rapidly to Deploy Readily Available Methane Mitigation Measures by Sector Can Immediately Slow Global Warming. *Environ. Res. Lett*. **2021**, 16 (5), 054042.

Roger, J.; Irakulis-Loitxate, I.; Valverde, A.; Gorroño, J.; Chabrillat, S.; Brell, M.; Guanter, L. High-Resolution Methane Mapping with the EnMAP Satellite Imaging Spectroscopy Mission. IEEE Trans. Geosci. *Remote Sens*. **2024**, 62, 1–12.

Sherwin, E. D.; Rutherford, J. S.; Zhang, Z.; Chen, Y.; Wetherley, E. B.; Yakovlev, P. V.; Berman, E. S. F.; Jones, B. B.; Cusworth, D. H.; Thorpe, A. K.; Ayasse, A. K.; Duren, R. M.; Brandt, A. R. US Oil and Gas System Emissions from Nearly One Million Aerial Site Measurements. *Nature* **2024**, 627 (8003), 328–334.

Thompson, D. R.; Leifer, I.; Bovensmann, H.; Eastwood, M.; Fladeland, M.; Frankenberg, C.; Gerilowski, K.; Green, R. O.; Kratwurst, S.; Krings, T.; Luna, B.; Thorpe, A. K. Real-Time Remote Detection and Measurement for Airborne Imaging Spectroscopy: A Case Study with Methane. *Atmos. Meas. Tech*. **2015**, 8 (10), 4383–4397.

Thorpe, A. K.; Frankenberg, C.; Aubrey, A. D.; Roberts, D. A.; Nottrott, A. A.; Rahn, T. A.; Sauer, J. A.; Dubey, M. K.; Costigan, K. R.; Arata, C.; Steffke, A. M.; Hills, S.; Haselwimmer, C.; Charlesworth, D.; Funk, C. C.; Green, R. O.; Lundeen, S. R.; Boardman, J. W.; Eastwood, M. L.; Sarture, C. M.; Nolte, S. H.; Mccubbin, I. B.; Thompson, D. R.; McFadden, J. P. Mapping Methane Concentrations from a Controlled Release Experiment Using the next Generation Airborne Visible/infrared Imaging Spectrometer (AVIRIS-NG). *Remote Sens. Environ*. **2016**, 179, 104–115.

Thorpe, A. K.; Green, R. O.; Thompson, D. R.; Brodrick, P. G.; Chapman, J. W.; Elder, C. D.; Irakulis-Loitxate, I.; Cusworth, D. H.; Ayasse, A. K.; Duren, R. M.; Frankenberg, C.; Guanter, L.; Worden, J. R.; Dennison, P. E.; Roberts, D. A.; Chadwick, K. D.; Eastwood, M. L.; Fahlen, J. E.; Miller, C. E. Attribution of Individual Methane and Carbon Dioxide Emission Sources Using EMIT Observations from Space. *Sci Adv* **2023**, 9 (46), eadh2391.

UNEP. Methane Alert and Response System (MARS). UNEP - UN Environment Programme. https://www.unep.org/topics/energy/methane/international-methane-emissions-observatory/methane-alert-and-response-system (accessed 2024-05-09).

Zandbergen, S. R.; Duren, R.; Giuliano, P. N.; Green, R. O.; Haag, J. M.; Moore, L.; Shaw, L.; Mouroulis, P. Optical Design of the Carbon Plume Mapper (CPM) Imaging Spectrometer. In Imaging Spectrometry XXV: Applications, Sensors, and Processing; Ientilucci, E. J., Bradley, C. L., Eds.; *SPIE*, **2022**. https://doi.org/10.1117/12.2633767.